Experimental characterization of Starch/beet-pulp Bricks for Building Applications: 1 Drying Kinetics and Mechanical Behavior

Georges Costantine, Elias Harb, Christophe Bliard, Chadi Maalouf, Elias Kinab, Fabien Beaumont, Guillaume Polidori

Experimental characterization of Starch/beet-pulp Bricks for Building Applications: Drying Kinetics and Mechanical Behavior

Georges Costantine[1], Elias Harb[1], Christophe Bliard[2], Chadi Maalouf[1], Elias Kinab[3], Boussad Abbès[1], Fabien Beaumont[1], Guillaume Polidori[1]

[1]Institut de Thermique, Mécanique et Matériaux, ITHEMM - EA 7548, Université de Reims-Champagne-Ardenne URCA, Moulin de la Housse, 51687 Reims Cedex 2, France
[2]Institut de Chimie Moléculaire de Reims, ICMR-UMR 7312 CNRS, Université de Reims-Champagne-Ardenne URCA, Moulin de la Housse, 51687 Reims Cedex 2, France
[3]Université Libanaise, Faculté de Génie, Branche II, Roumieh, Liban

Abstract

Buildings account for a large share of the primary energy and materials use in Europe. Therefore, the EU has set several energy and materials targets for the built environment and other sectors. Novel low-carbon materials can play a major role in the transition towards meeting those targets. Moreover, agriculture produces by- or waste products that could be used as constituent of innovative agro-materials for construction. Recently, beet pulp based-material is being investigated on the material scale and promising results are pointed out regarding its interesting mechanical, hygrothermal and acoustical properties for building insulation use. In this context, the paper aims to study experimentally two types of beet-pulp starch composites: whole bricks and hollowed bricks. The manufacturing of the two types of bricks is detailed. A comparative study is then achieved regarding the drying kinetics, mechanical properties as well as internal structure composition.

Keywords: beet-pulp, starch, brick, drying kinetics, SEM, mechanical properties.

I. Introduction

Over the last century, the extraction of building materials and fossil fuels has been multiplied by 34 and 12, respectively (CREE 2015). Thus, concrete is the second most consumed material in the world after water. The sand, one of concrete constituent, is the second extracted mineral raw material with a shortage announced as the same level as fossil fuels with numerous environmental and socio-economic impacts. On the other hand, according to the last report of the World Meteorological Organization WMO (September 2019), the period between 2015 and 2019 is set to be the warmest five-year period on record,

compared to the years 2011 – 2015. In the same context, the WMO report on greenhouse gas concentrations shows that 2015 – 2019 has seen a continued increase in carbon dioxide (CO_2) levels and other key greenhouse gases in the atmosphere to new records, with CO_2 growth rates nearly 20 % higher than the previous five years ((WMO) 2019). Therefore, the worries about climate change consequences and the awareness of the mineral resources shortage have pushed several countries to put in place policies encouraging the deployment of a bio-sourced economy based on the extraction and exploitation of the biomass.

The building sector is one of the fields witnessing a significant transition towards eco-friendly materials. As a matter of fact, the building sector in Europe is responsible for 25 % of the total energy consumption and 11 % of all greenhouse gas emissions, as stated in the report of the European Commission in 2013 (European Commission 2013). In France, it is classified as the first energy consuming (43 %) and second contributor to CO_2 emissions (25 %), just behind the transportation sector (ADEME 2013). Consequently, France has engaged through national and European commitments to improve the energy efficiency of its building sector, for instance, the Climate and Energy Package in 2008 (Paquet Climat-Energie 2008), the Grenelle 1 Environment Law in 2010 (Grenelle 1 Enivronnement 2010), the Thermal Regulation RT of 2012 (RT 2012) and the adoption of the Energy Transition for Green Growth Act in 2015 (LTECV 2015). Moreover, recently, France has drawn up the National Low Carbon Strategy (SNBC) introducing the “BBCA” (low carbon buildings) label (BBCA 2018). The main objective of this new reference is to propose a carbon footprint assessment methodology for existing buildings. It involves also low carbon initiatives, halving CO_2 emissions and highlighting best practices and operations to reach this goal. In the same vein, this energy transitions is accompanied by the new Responsible Building Regulation RBR 2020 – 2050 (RBR and RBR 2020-2050 2015), in which sustainable buildings have to respect the requirements of the “BEPOS” label (Positive Energy Building) leading to the concept of “self-sufficient buildings”.

Therefore, taking energy efficiency measures into account in new and renovated dwellings will result in a higher demand for thermal insulation which is fundamental to improve the housing comfort by reducing thermal losses through the building envelope. In this context, developing innovative materials for construction is one of the most interesting solutions nowadays. The main target is to contribute significantly to the storage of atmospheric carbon and the preservation of natural resources as well as to change in building

consumption behavior. In addition, focusing on local renewable resources makes these products affordable in terms of elaboration and transportation fees.

A review of the literature shows a whole range of plant aggregate based materials (Mnasri et al. 2020): hemp concrete, cork and straw based products (Douzane et al. 2016), wood, crop based materials such as typha-Australis (Niang et al. 2018), date palm fibers and beet-pulp fibers (Belakroum et al. 2017) … Recent studies describe the elaboration and characterization of a new agro-composite based on sugar beet pulp and potato starch as a bio-sourced binder (Karaky et al. 2018). Different compositions (ratio of starch/pulp) designed for building thermal insulation are tested. Accordingly, mechanical, acoustical and hygrothermal characterization show that the ratio of 0.4 represents the optimal composition as thermal insulator (Karaky 2018). However, these bio-based products are generally hygroscopic porous materials and continuously subjected to imbibition–drying cycles which seriously affect their durability, in terms of chemical alterations of the structure (Shahidzadeh-Bonn et al. 2007). As a result, the moisture content within the material depends not only on the water absorbed but also on the amount of water released by evaporation mechanism, which is described by the drying process. Thus, investigating the materials drying kinetics is useful in understanding the effect of environmental conditions on the moist storage of building materials (Karoglou et al. 2005). Literature provides numerous studies dealing with drying kinetics, as for instance the effects of wetting properties in the drying of porous media (Shahidzadeh-Bonn et al. 2007), the influence of hydraulic contact interface on the drying of masonry walls (Delgado et al. 2019), the impact of boundary conditions and water retainers on delaying the drying process within hemp concrete blocks (Glouannec et al. 2010) …

Based on the above findings, the aim of this paper is to compare two types of starch - beet-pulp (SBP) fiber composite for wall and floor applications: full brick and hollowed brick. The composition of starch/pulp equal to 40 % is considered in this study. Two types of beet-pulp brick specimens were manufactured. The drying kinetics of each type were studied experimentally and analytically. Then, their mechanical properties were measured and compared. The preliminary results show that drying kinetics respect mathematical models provided by the literature. Moreover, Mechanical tests point out interesting properties for hollowed bricks in terms of compressive strength and elastic modulus.

II. Experimental set-up

II.1 Molds manufacturing

Two types of wood molds were used for bricks manufacturing. The first one (Figure 1) designed for full bricks is of dimensions (L = 23.3 cm, w = 11 cm and h = 7.4 cm) with a fitted wood piston or cover of (L' = 23.3 cm, w' = 11 cm and h' = 1.8 cm) which makes the content volume equivalent to $V_1 = 1435.28 \times 10^{-6}$ m^3. The second type is shown in Figure 2 for hollowed bricks of same dimensions but with copper tubes of diameter Ø = 1.8 cm leading to inner content volume of $V_2 = 1193.02 \times 10^{-6}$ m^3. The wooden piston role is to compact the mixture inside the mold and to contribute to have flat surfaces of the specimens.

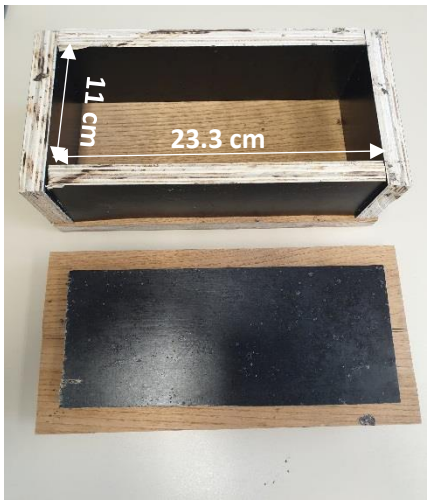

Figure 1 : Mold used for full bricks manufacturing

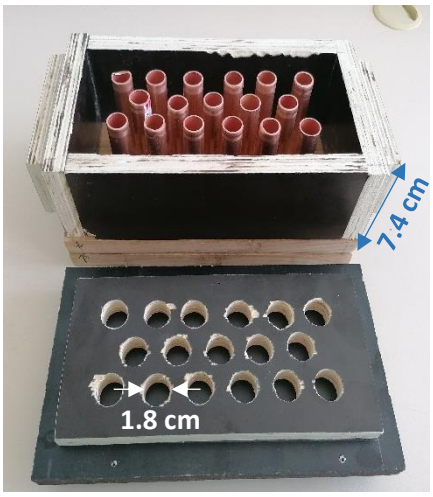

Figure 2 : Mold used for hollowed bricks manufacturing

II.2 Specimen preparation

Based on Karaky PhD thesis (Karaky 2018) work which studied four compositions of SBP (10 %, 20 %, 30 % and 40 % starch), the ratio of 40 % of starch with respect to the total pulp mass was considered as the optimal composition from mechanical, acoustical and hygrothermal properties point of view. Consequently, only the starch/pulp ratio of 0.4 was used in specimen manufacturing in this work.

Since both starch and beet pulp are very hydrophilic, beet pulp pellets were first soaked separately during two hours with distilled water to reach their saturation degree with a water/pulp mass ratio equal to 2.5. *Figure 3*, *Figure 4* and *Figure 5* show the volume of pulp granulates before, after and during water immersion, respectively. The mass of beet pulp m_p

and starch powder m_s are calculated as follows: knowing the dry density of the material for the chosen composition (ρ = 360 kg.m^{-3}) and the volume of the molds (V_1 = 1435.28 × 10^{-6} m^3 and V_2 = 1193.02 × 10^{-6} m^3), the mixture (beet and starch) mass m is obtained. Therefore, the necessary quantity of beet pulp is calculated based on equation **(1)**:

$$m = m_p + m_s$$
$$m_s = 0.4\, m_p \qquad (1)$$

Figure 3 : Beet pulp pellets before water immersion

Figure 4 : Beet pulp fibers after immersion in water

t = 0 min t = 10 min t = 30 min

Figure 5 : Pulp pellets swelling in water

In the next step, potato starch powder was added to the saturated wet pulps and mixed manually for 10 minutes until an homogeneous admix was obtained. The pulp, initially greenish, became yellowish after adding starch. The obtained mixture was then placed in an autoclave and heated for 30 minutes at 120 °C to jellify starch granules (*Figure 6*). The produced hot water vapor dissolves the starch, which transforms into a gluey texture. Once the starch dissolves completely, the mixture can finally be poured into the wooden molds (*Figure 7*). The beet pulp-starch mixture is then compacted under a pressure of 0.044 MPa. Greaseproof papers were placed in the molds to facilitate the removal of the sample. *Figure 8* and *Figure 9* show a full and a hollowed brick, respectively. The samples were frozen at -80°C before drying. The drying methods and kinetics are discussed in details in the next section.

Figure 6 : Mixture heating in an autoclave

Figure 7 : Mixture poured in wooden molds

Figure 8 : Full brick specimen

Figure 9 : Hollowed brick specimen

II.3 Drying process

The brick drying process is the last phase of the experimental set-up. Physically, it is a complex phenomenon driven by heat and mass transfers inside and on the surface of the material. In addition, the drying mechanism depends strongly on other nonlinear physical phenomena including stress distribution and cracks emergence in the material (Gualtieri et al. 2016). The mass transport mechanism during the drying process is triggered by the humidity gradient between the material surface and its wet core. The mechanisms of mass transport are related to various phenomena: internal pure diffusion, surface diffusion, Knudsen diffusion, capillary flow, evaporation, condensation and thermal diffusion (Chemkhi and Zagrouba 2008). Therefore, the drying process described previously results in dimensional changes of the specimen, called shrinkage. In this work, two drying methods are studied:

through pulsed hot air drying tower and freeze drying. The optimal one was chosen based on lower shrinkage volume and the surface quality of the sample (cracks emergence). The drying procedure consisted in monitoring the samples masses using an electronic balance of ± 0.01 g accuracy until stabilization was reached. Initially, the weighting time interval is 10 minutes and increased to 30 minutes at the end to avoid disturbance of the drying process when mass variation was very low. The drying monitoring were stopped when four successive measurements of the brick masses differences were under 0.1 g.

II.3.1. Pulsed hot air drying tower

In this drying method, a hot air drying tower with a temperature of 40 °C was used as shown in *Figure 10* and *Figure 11*. The ambient air entering the oven through the vent was heated up prior to circulating around the samples. This setup allows to heat the enclosure from bottom to top and to dry the brick evenly.

Figure 10 : Hot air drying tower

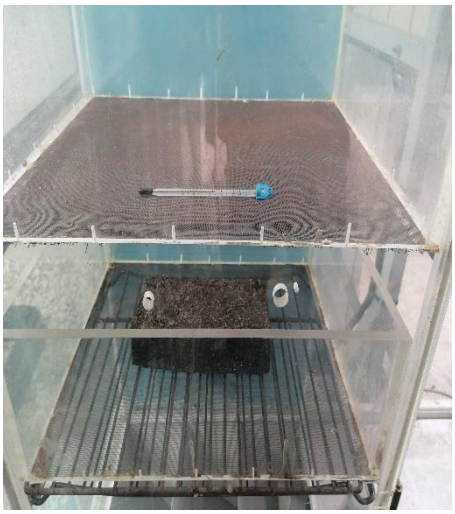

Figure 11 : Brick sample in the drying tower

II.3.2. Freeze drying

Figure 12 : Lyophilizer used for sublimation

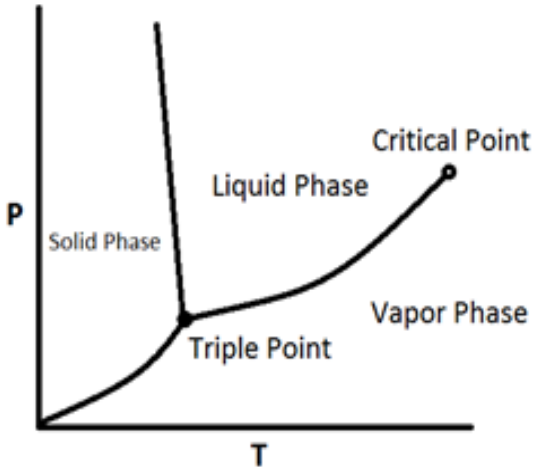

Figure 13 : Pressure-temperature diagram

Lyophilization phenomenon combines the action of cooling and vacuum to achieve the sublimation of ice crystals without going through the liquid phase. Freeze drying is a third generation drying technology which has four distinct stages: freezing, vacuum, sublimation and crystallization of the water vapor. It has proved to help overcome issues related to structural damage of the end product (Karel 1975) (Dalgleish 1990) due to the fact that the absence of air prevents oxidative deterioration as well as the possibility of heat damage. The samples are cooled rapidly to low temperatures reaching -80 °C to obtain small ice crystals (the subsequent sublimation is then facilitated). The pressure is then lowered below the triple point (*Figure 13*) to allow the sublimation of crystals. Thus, the formation of intermediate liquid water is avoided. Sublimation continues to dry the product as long as a 200 – 300 Pa pressure range is maintained.

II.4 Drying Kinetics

II.4.1. Experimental results

The efficiency of the drying procedure was assessed based on the shrinkage percentage of the material and the quality of the sample surfaces after the drying in terms of cracks emergence. The dimensions of the specimen were measured before and after the drying process and the shrinkage percentage was calculated as follows in equation **(2)** and showed in the *Table 1*:

$$S = \frac{V_i - V_f}{V_i} \times 100 \qquad (2)$$

Where V_i and V_f are initial (before drying) and final (after drying) specimen volumes, respectively.

Drying method	Shrinkage percentage (%)
Hot air drying tower	28,7
Liophilizer	2,5

Table 1 : Shrinkage percentage per drying method

Figure 14 : Brick sample dried with the ventilated oven

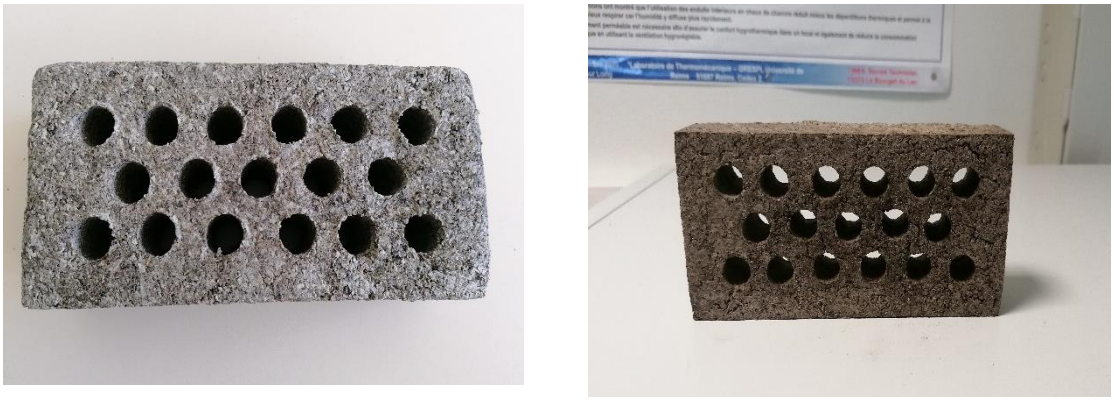

Figure 15 : Brick sample dried with lyophilizer

In addition, the figures above (*Figure 14* and *Figure 15*) show the quality of the samples surface after the drying process using different methods. The results showed that the freeze-dried bricks show the lowest shrinkage percentage and a more homogeneous surfaces on all brick sides as compared to other drying methods which resulted in more irregular brick shapes on which micro-cracks could be seen.

II.4.2. Experimental drying kinetics

The drying kinetics are presented in *Figure 16* and *Figure 17* as mass loss of the samples as a function of time. The evolution of moisture ratio for 3 full bricks and 3 hollowed bricks are presented in *Figure 16* and *Figure 17*. The moisture ratio shown is calculated using equation **(3)**:

$$\textit{Moisture ratio} = \frac{m(t) - m_f}{m_0 - m_f} \qquad (3)$$

Where m(t) is the sample mass at an instant t, m_f represents its final mass at the end of the drying (equilibrium mass) and m_0 the initial mass at t=0.

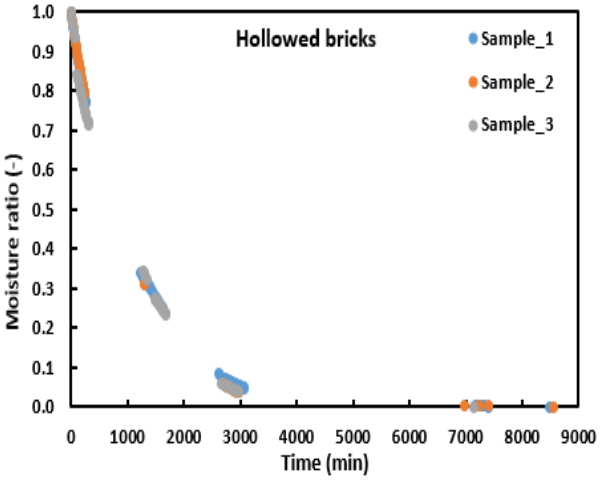

Figure 16 : Drying kinetics (moisture ratio vs time) for 3 hollowed bricks

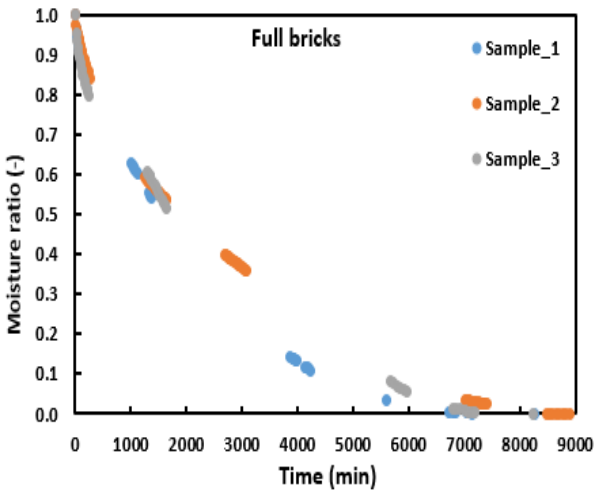

Figure 17 Drying kinetics (moisture ratio vs time) for 3 full bricks

The comparison of *Figure 16* and *Figure 17* shows that for hollowed bricks, mass stabilization is reached by 3500 min (approximately 2 to 3 days) while full bricks need almost 7500 min (approximately 5 to 6 days) to reach their dry mass. This result is correlated with the mass and heat transfer between the air and the brick surface. Hollowed bricks present a much more important interaction surface with the surrounding air, which leads to faster drying. In other words, the shape of hollowed brick with holes gives the water a large number of channels to leave the sample. In addition, the results shown in *Figure 16* are very close for the three perforated bricks whilst the results in *Figure 17* present a much larger deviation between the curves. This is mainly due to the holes, which allow a better air circulation on the surface and within the samples, while in the whole bricks, the drying begins on the surfaces and does not reach uniformly the core of the specimen.

II.4.3. Simulation of the drying process via ANSYS Fluent

Generally, the evaporation process of a material is invisible and it is difficult to determine how moisture transfer is distributed. However, it is possible to simulate mass transfer process within materials using computational fluid dynamics (CFD). For a better understanding, the drying process of the bricks is simulated using the ANSYS Fluent 19.2 calculation code based on the finite volume method. The Eulerian multiphase model is coupled with an evaporation model so that the liquid phase is evaporated from the brick (modelled as a porous material), simulating the drying process. The Lee model (Lee 1979) which is a mechanistic model with a physical basis is used in the simulation. In the evaporation model of Lee, the mass transfer between the liquid and the vapor (evaporation and condensation) is governed by the vapor transport equation:

$$\frac{\partial}{\partial t}(\alpha_v \rho_v) + \nabla \cdot \left(\alpha_v \rho_v \vec{V}_v\right) = \dot{m}_{lv} - \dot{m}_{vl} \qquad (4)$$

Where v represents the vapor phase, α_v the volume fraction, ρ_v the vapor density, $\vec{V}_v$ the vapor phase velocity and $\dot{m}_{lv}, \dot{m}_{vl}$ are respectively the rates of mass transfer due to evaporation and condensation ($kg.m^{-3}.s^{-1}$). The water-saturated brick is virtually placed in an oven in which hot air circulates, causing the liquid phase contained in the brick to evaporate. The oven drying method was chosen for the CFD simulations since it is the most representative for the phenomenon. *Figure 18* and *Figure 19* show the results of the CFD simulations. It can be noticed that the air flows through the holes of the hollowed brick facilitating the drying process unlike the case of the whole brick where the air passes around the sample, leading to high relative humidity (higher than 82 %) within the brick.

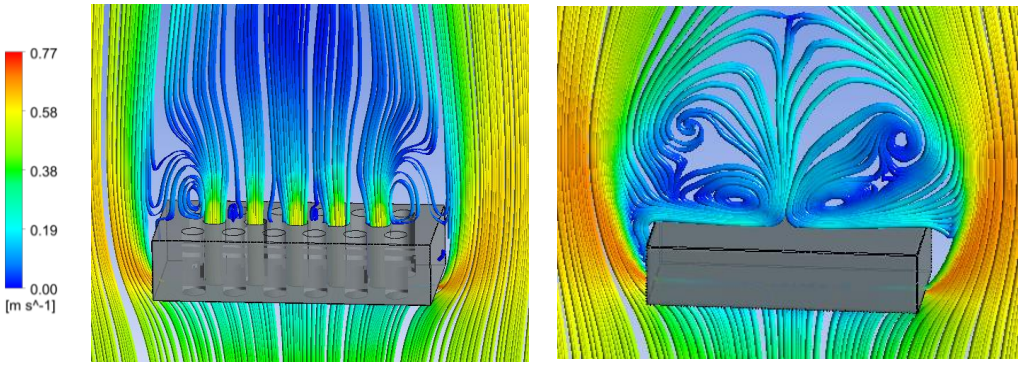

Figure 18 : Streamlines colored by velocity of the flow inside the drying oven for the hollowed and full brick.

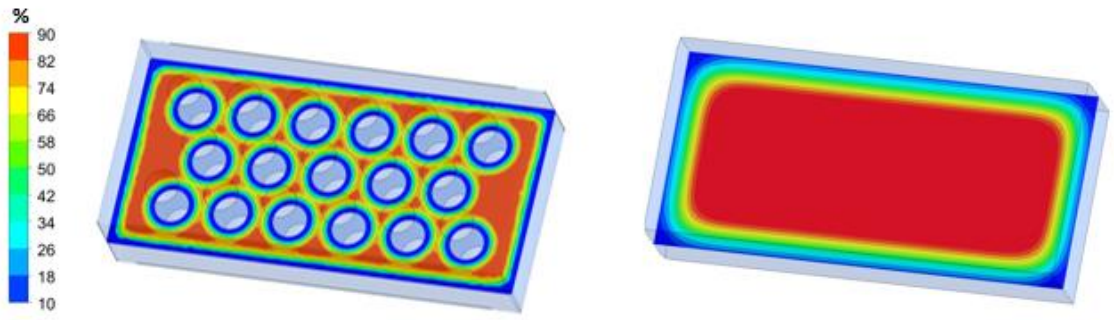

Figure 19 : Relative humidity (%) in the horizontal center plane of the whole and hollowed brick at t=12 hours after the start of the drying process.

II.4.4. Mathematical approaches for drying kinetics modelling

Literature provides different analytical models describing the drying process applied on fruits, vegetables, agriculture and crop-based products (Onwude et al. 2016). The main categories can be distinguished: theoretical, semi-theoretical, and empirical models. The theoretical ones are difficult in application in comparison with semi-theoretical and empirical approaches. The semi- theoretical ones are based on a compromise between theory and ease of application (Hii et al. 2009). They are generally derived from Fick's second law such as Henderson and Pabis, Logarithmic, Midilli and Kucuk and two terms exponential models or derived from Newton's law of cooling and its modifications such as Newton, Page and Page modified models. Finally, the empirical models establish a direct relationship between the water content of the material and the drying time by means of regression analysis such as parabolic models (Taghian Dinani et al. 2014) . The major limitation of empirical models in the drying is that they do not have a physical interpretation since they are basically derived from experimental data and generally don't follow the theoretical fundamentals of drying processes in the form of a kinetic relationship between the rate constant and the moisture concentration (Onwude et al. 2016). In this work, a comparison between semi-theoretical models is established (*Table 2*).

Model	Equation	References
Newton	$\mathbf{MR = exp(-Kt)}$	(Ayensu 1997)
Page	$\mathbf{MR = exp(-Kt^n)}$	(Karathanos and Belessiotis 1999)
Page modified	$\mathbf{MR = exp(-Kt)^n}$	(Vega et al. 2007)
Henderson and Pabis	$\mathbf{MR = a\ exp(-Kt)}$	(Akpinar et al. 2003)
Logarithmic	$\mathbf{MR = a\ exp(-Kt) + c}$	(Yaldiz et al. 2001)

Two terms exponential	$\mathbf{MR = a\,exp(-Kt) + (1 - a)exp(-Kat)}$	(Akpinar et al. 2003)
Midilli Kucuk	$\mathbf{MR = a\,exp(-Kt^n) + bt}$	(Midilli et al. 2002)

Table 2 : Semi-theoretical models used for drying process

Drying kinetics are evaluated describing the weight loss of the brick sample with time as shown in equation (3). The results of the sample_3 drying mechanism (whole and hollowed bricks) are fitted using the models of Table 2 based on least squares method. Calibration constants as well as correlation coefficients and root mean square errors are listed in *Table 3* and *Table 4* below. Fitted models are shown in *Figure 20* and *Figure 21* for each brick type.

Models	Parameters	R2	RMSE
Newton	K = 0.000429	0.991887	0.056464
Page	K = 0.000751, n = 0.926990	0.990525	0.055427
Page modified	K = 0.000457, n = 0.937004	0.991887	0.056464
Henderson and Pabis	K = 0.000380, a = 0.926582	0.995041	0.038286
Logarithmic	K = 0.000380, a = 0.926579, c = 0	0.995040	0.038286
2 terms-exponential	K = 0.008082, a = 0.049548	0.992984	0.047036
Midilli-Kucuk	K = 0.000054, a = 0.894308, n = 1.246693, b = 1×10^{-10}	0.996836	0.028026

Table 3: Fitting parameters of the calibration models for the whole brick

Models	Parameters	R2	RMSE
Newton	K = 0.000943	0.996395	0.035386
Page	K = 0.002064, n = 0.890823	0.996778	0.028095
Page modified	K = 0.000967, n = 0.890827	0.996778	0.028095
Henderson and Pabis	K = 0.000885, a = 0.952857	0.997033	0.026829
Logarithmic	K = 0.000885, a = 0.952857, c = 0	0.997033	0.026829
2 terms-exponential	K =0.011587, a = 0.074274	0.997832	0.023353
Midilli-Kucuk	K = 0.970773, a = 0.961979, n = 0.001106, b = 0	0.997085	0.026712

Table 4: Fitting parameters of the calibration models for the hollowed brick

The global observation shows that all the prediction models show satisfactory fits for the experimental drying curves. However, the drying kinetics are predicted with lower deviation from experimental measurements for the case of hollowed bricks since a higher coefficient of correlation R2 and a lower RMSE are obtained. This finding is in good agreement with previous conclusions stating that drying phenomenon for hollowed bricks is more homogeneous and efficient. Moreover, according to Glouannec et al. (2010) in their work on the drying of hemp-lime blocs, the impact of water diffusion through a porous material is probably more restrictive on the drying kinetics than the evaporation at the surface. The water diffusion is probably enhanced within the core of hollowed bricks and results in an improved drying in this case.

In addition, Newton, Page and Page modified models show higher deviations with the experimental moisture ratio than the semi-theoretical models based on Fick's law which seems more appropriate than Newton's law of cooling and its modifications to describe the drying process. Moreover, in the literature, it has been proved that Newton exponential model shows some limitations in this field and doesn't provide accurate simulation of drying curves at early and later stages during drying mechanism (Sogi et al. 2003)(Simal et al. 2005). The drying curves are well predicted with Middili Kucuk and two terms exponential for the hollowed brick and with Midilli Kucuk for whole brick case.

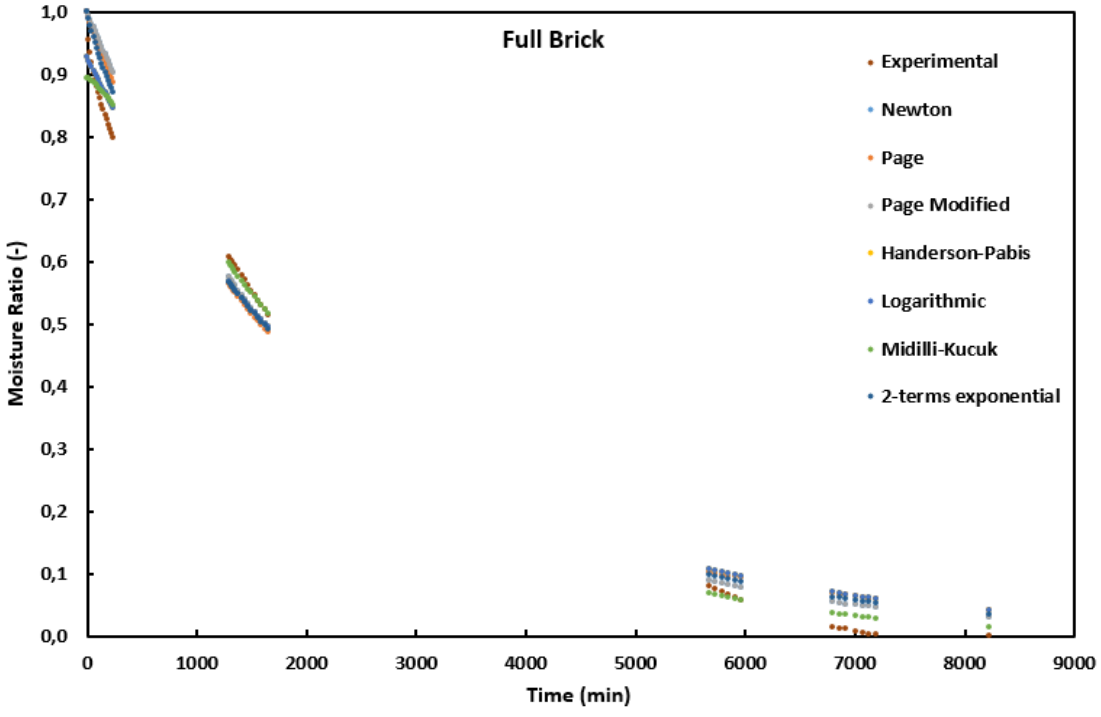

Figure 20 : Fitting model for the drying curve of a whole brick

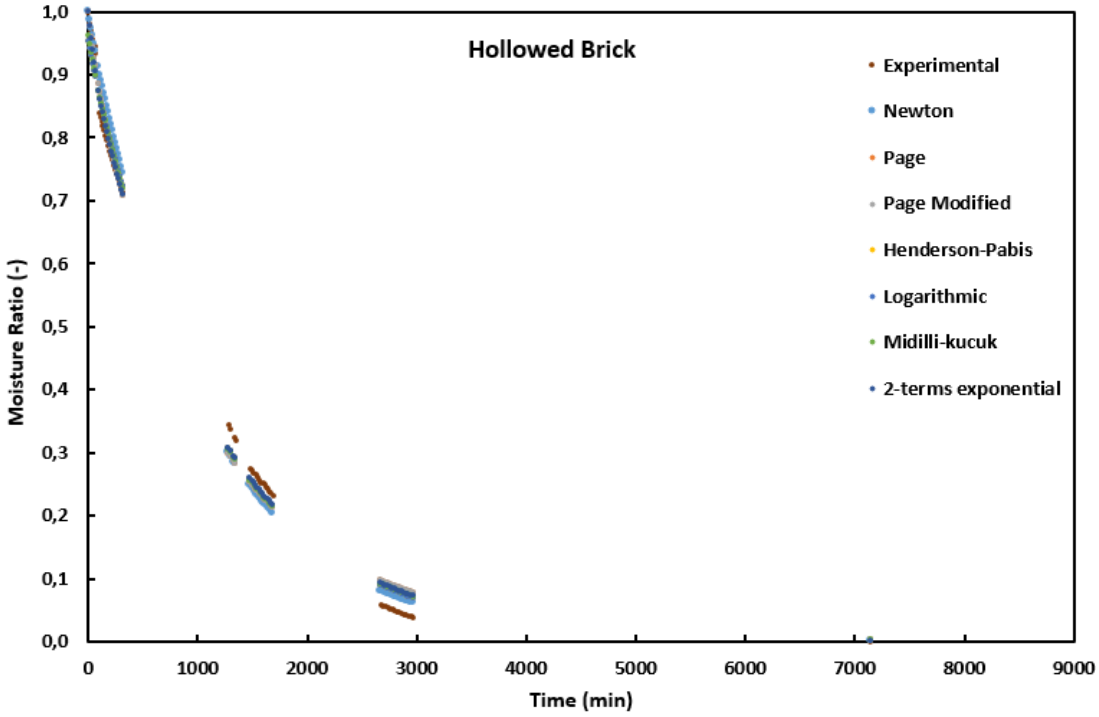

Figure 21 : Fitting model for the drying curve of a hollowed brick

III. Experimental characterization of beet-pulp bricks

III.1 Microstructure analysis

The microstructure analysis of starch, beet pulp, as well as the wet and dry mixture was done using the scanning electron microscope (SEM) method. Three specimens were tested as listed in *Table 5*. The experimental procedure consists in scanning the specimen surface with a focused beam of electrons, which interact with the atoms of the sample. The latter interaction produces various signals that contain information about the surface topography and composition of the sample.

Specimens	Constituents
Spec. 1	Native starch granules
Spec. 2	Beet-pulp
Spec. 3	Mixture of starch/beet-pulp

Table 6: Specimens tested using the scanning electron microscope

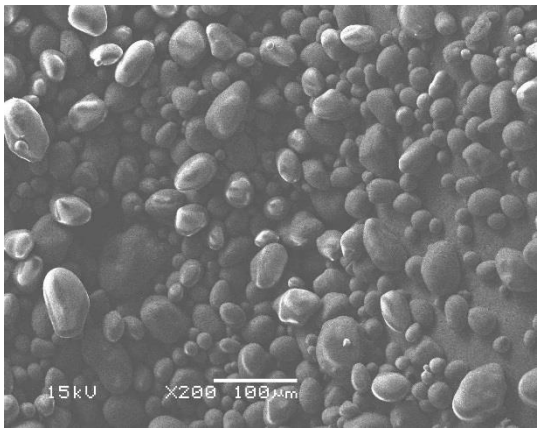

Figure 22: Dry native starch granules with a x200 zoom

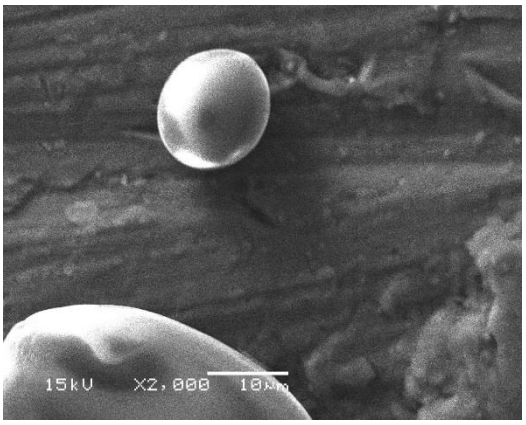

Figure 23 : Dry native starch granules with a x2000 zoom

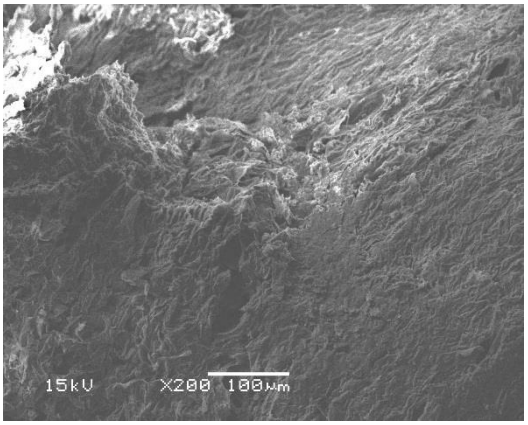

Figure 24: Dry beet-pulp with a x200 zoom

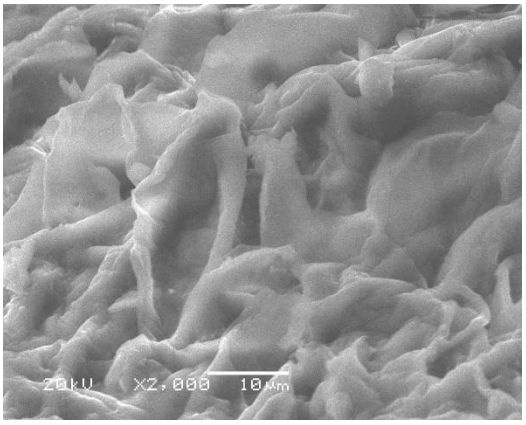

Figure 25: Dry beet-pulp with a x2000 zoom

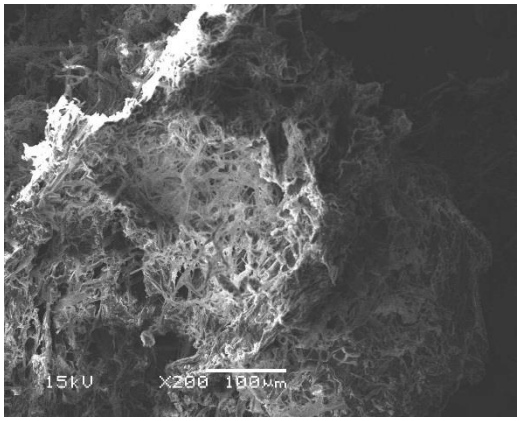

Figure 26: Starch and beet-pulp mixture with a x200 zoom

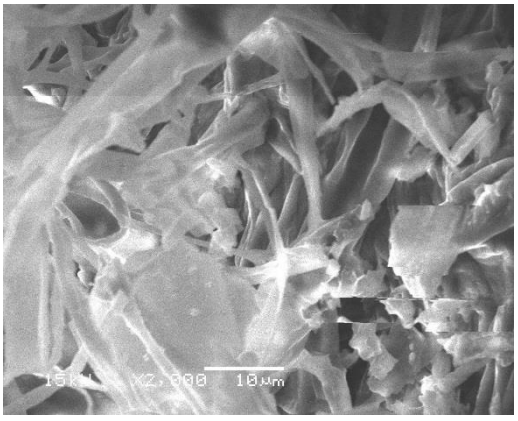

Figure 27 : Starch and beet-pulp mixture with a x2000 zoom

286 *Figure 22* and *Figure 23* show native potato starch granules with 10-300 µm size. *Figure 24* and
287 *Figure 25* show the structure of dried rehydrated beet pulps with a spongy appearance. This
288 structure corresponds to the remains of the plant cell structure, destructured during the

process of sugar extraction. On these pictures, the plant fibers appear irregular. *Figure 26* and *Figure 27* show the prepared SBP composite homogeneously mixed and autoclaved. The starch granules cannot be seen any longer and the beet pulp spongy structure seems to have been replaced by a more rugged and open structure. This indicates a good compatibility between the two polymeric constituents.

III.2 Mechanical compression test

Compression tests were conducted on two specimens from each brick type. These tests respect the international standards organization ISO 527-4 (ISO527-4 1997) under indoor conditions of 23 °C ambient temperature and 50 % relative humidity with a rate of 10 mm/min (Khalfallah et al. 2014). A Digital Image Correlation (DIC) measurement tool is set with an Instron 33R 4204 testing machine equipped with 50 kN loading cell. Two Charge-Coupled Device (CCD) cameras permit to take images recording the deformation during the tests. The ARAMIS sensor is a stereo camera system providing precise 3D coordinates based on triangulation (Aramis 2009) (*Figure 28 (a)*). Digital gray scale pictures of the surface were taken every second during compression test. These images were used as input to calculate the displacement field using the DIC method. Compression tests were always performed in the compacting pressure direction, as shown in *Figure 28 (b)* and *(c)*.

(a)

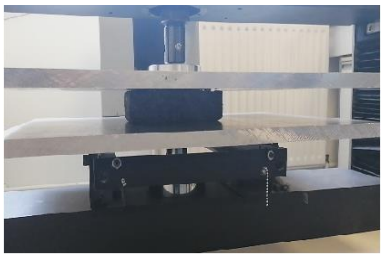

(b)

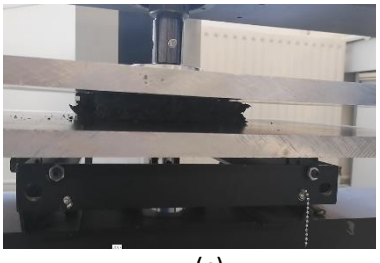

(c)

Figure 28 : Experimental set-up of the compression test: (a) ARAMIS sensor, (b) Brick before compression, (c) Brick after compression.

Typical cartographies of major engineering strains under compressive test are shown in *Figure 29* and *Figure 30* for whole and hollowed bricks, respectively. For the case of whole bricks, the first crack was observed from the brick top surface after 10 seconds only. This crack propagates through the brick and with increasing load another crack appears and propagates from the brick's bottom surface. When the deformation reaches 13 % at around 50 s, the brick becomes totally damaged (*Figure 29 (c)*).

The hollowed brick shows higher compression resistance. The first cracks were only observed on the bottom surface and bottom right corner after 45 s (*Figure 30 (a)*). *Figure 30* shows that the crack on the bottom right corner propagates and reaches the top surface when the brick is totally damaged reaching a deformation of 17 % after 130 s of testing (*Figure 30 (c)*). These findings are in compliance with the curves in *Figure 31* and *Figure 32* showing the compression load versus displacement for whole and hollowed bricks, respectively. The maximum observed compression load was 3.75±0.75 kN for the whole brick, but it reached 13.0±1.0 kN for the hollowed one.

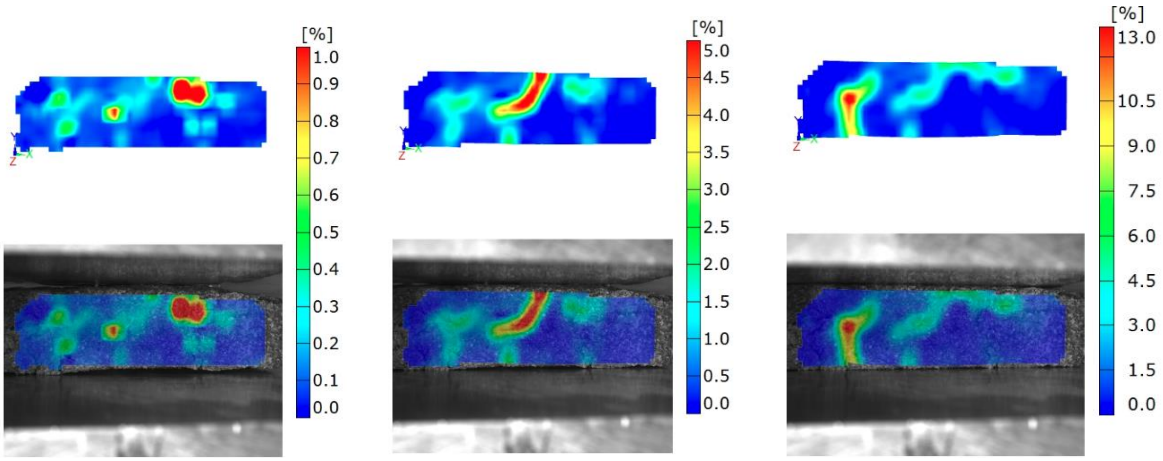

(a) – 10 s *(b) – 29 s* *(c) – 50 s*

Figure 29 : Cartographies of engineering strains (in %) under compressive load obtained by ARAMIS method for whole bricks at 10 s, 29 s and 50 s

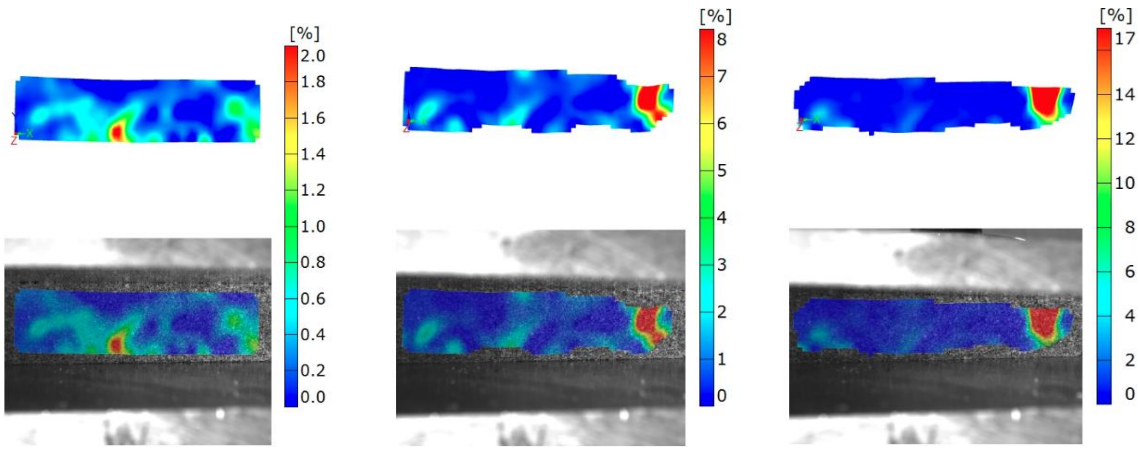

(a) – 45 s *(b) – 91 s* *(c) – 130 s*

Figure 30 : Cartographies of engineering strains (in %) under compressive load obtained by ARAMIS method for hollowed bricks at 45 s, 91 s and 130 s

323

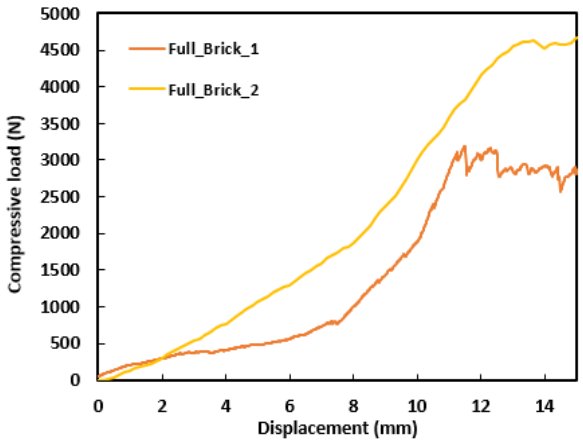

Figure 31 : Compression load-displacement curves for full bricks

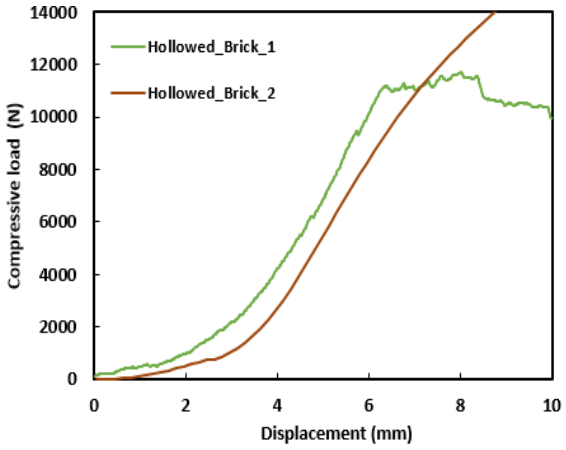

Figure 32 : Compression load-displacement curves for hollowed bricks

324

325 The results are in agreement with Schellbach (1971) findings showing that much stronger walls
326 are given by bricks with vertical perforations and when these cavities do not exceed 35% of
327 the cross-section, the bricks behave as if solid. However, such increase in the loadbearing is
328 not only due to structure of the brick, but can be linked to the efficiency of the drying process
329 in the hollowed bricks, while whole bricks would generate mold in the core of the structure,
330 directly affecting its mechanical behavior. In addition, considering the elasticity zone, an
331 average value of the Elastic modulus was calculated for each brick type. The obtained values
332 are 2.15±0.20 MPa and 8.14±0.8 MPa for whole and hollowed bricks, respectively, showing
333 that hollowed bricks can be used as a rigid material for building application. These values are
334 comparable with previous studies: effectively, Karaky et al. (Karaky et al. 2019) found an

335 average elasticity modulus of Starch-Beet Pulp composite ranging between 2.06 MPa and 3.17
336 MPa depending on the starch to Beet-pulp ratio. Moreover, in their study on starch-hemp
337 material, Bourdot et al. (Bourdot et al. 2017) obtained an elastic modulus between 2.14 MPa
338 and 2.47 MPa based on starch-hemp ratio. Therefore, the compressive test results highlight
339 the competitive mechanical properties of hollowed bricks for construction use.

340 ## IV. Conclusions

341 This work deals with the experimental characterization of a new bio-sourced building
342 insulation material based on starch and beet pulp. Two types of bricks were manufactured
343 and tested: full bricks and hollowed bricks. The investigations were conducted on the drying
344 kinetics of each type and their mechanical behaviour regarding compressive tests comparison.
345 The results show that the drying process using a lyophilizer provide a more effective drying
346 regarding the shrinkage percentage and the sample surface quality after the drying. In
347 addition, it has been proved that the hollowed bricks drying is faster and more homogeneous
348 thanks to air tube channels within the core of the specimen. The drying kinetics for both types
349 were mathematically investigated and succeeded to be modelled via semi-theoretical models
350 especially Middili Kucuk and two terms exponential models. Moreover, the microstructure
351 analysis of the beet-pulp composite shows a homogeneous mixture and a good compatibility
352 between the polymeric constituents starch and beet-pulp. On the other hand, mechanical
353 compressive tests were conducted on each brick type. Results show that the hollowed bricks
354 present a better resistance to compression load resulting in a higher elasticity modulus which
355 give them interesting mechanical properties in building applications. The number and the
356 shapes of the perforations can be optimised to obtain optimal overall performances by
357 increasing mechanical properties (Hollow Brick Masonry, 2008) in order to define the
358 compatible applications in building, such as roof or walls (non load bearing structures). Further
359 investigations using starch/beet-pulp hollowed bricks are also ongoing at wall scale to study
360 the hygrothermal behaviour of this material.

361 ## V. Acknowledgment

362 The authors would like to thank Crystal Union Company for providing the beet-pulp
363 necessary for the specimens manufacturing.

364 ## VI. References

(WMO), World Meteorological Organization. 2019. *WMO Provisional Statement on the State of the Global Climate in 2019*. WMO. Geneva: WMO.

ADEME. 2013. “Les Chiffres Clés Du Bâtiment Énergie - Environnement.” http://www.ademe.fr/sites/default/files/assets/documents/chiffres-cles-batiment-edition-2013-8123.pdf.

Akpinar, Ebru Kavak, Yasar Bicer, and Cengiz Yildiz. 2003. “Thin Layer Drying of Red Pepper.” *Journal of Food Engineering* 59 (1): 99–104. https://doi.org/10.1016/S0260-8774(02)00425-9.

Aramis. 2009. “User Manual Software V 6.1, Operating System | Deformation (Mechanics).” https://www.scribd.com/document/361218041/aramis-v6-1-pdf.

Ayensu, Akwasi. 1997. “Dehydration of Food Crops Using a Solar Dryer with Convective Heat Flow.” In *Solar Energy*, 59:121–26. Elsevier Science Ltd. https://doi.org/10.1016/S0038-092X(96)00130-2.

BBCA. 2018. “BBCA.” 2018. https://www.batimentbascarbone.org/label-bbca/.

Belakroum, R., A. Gherfi, K. Bouchema, A. Gharbi, Y. Kerboua, M. Kadja, C. Maalouf, T. H. Mai, N. El Wakil, and M. Lachi. 2017. “Hygric Buffer and Acoustic Absorption of New Building Insulation Materials Based on Date Palm Fibers.” *Journal of Building Engineering* 12 (July): 132–39. https://doi.org/10.1016/j.jobe.2017.05.011.

Bourdot, Alexandra, Tala Moussa, Alexandre Gacoin, Chadi Maalouf, Patricia Vazquez, Céline Thomachot-Schneider, Christophe Bliard, et al. 2017. “Characterization of a Hemp-Based Agro-Material: Influence of Starch Ratio and Hemp Shive Size on Physical, Mechanical, and Hygrothermal Properties.” *Energy and Buildings* 153 (October): 501–12. https://doi.org/10.1016/j.enbuild.2017.08.022.

Chemkhi, S., and F. Zagrouba. 2008. “Development of a Darcy-Flow Model Applied to Simulate the Drying of Shrinking Media.” *Brazilian Journal of Chemical Engineering* 25 (3): 503–14. https://doi.org/10.1590/S0104-66322008000300008.

CREE, Archietctures. 2015. “Architectures CREE.” *N°373*, 2015.

Dalgleish, J. McN. (J. McNair). 1990. *Freeze-Drying for the Food Industries*. Elsevier Applied Science, New York.

Delgado, J. M.P.Q., A. C. Azevedo, and A. S. Guimarães. 2019. “Influence of Hydraulic Contact Interface on Drying Process of Masonry Walls.” *Drying Technology* 38 (9): 1–17. https://doi.org/10.1080/07373937.2019.1615939.

Douzane, Omar, Geoffrey Promis, Jean Marc Roucoult, Anh Dung Tran Le, and Thierry Langlet. 2016. “Hygrothermal Performance of a Straw Bale Building: In Situ and Laboratory Investigations.” *Journal of Building Engineering* 8 (December): 91–98. https://doi.org/10.1016/j.jobe.2016.10.002.

European Commission. 2013. “EU ENERGY, TRANSPORT AND GHG EMISSIONS, TRENDS TO 2050, REFERENCE SCENARIO 2013.” Luxembourg. https://doi.org/10.2833/17897.

Glouannec, P., P. Chauvelon, and T. Colinart. 2010. “Experimental and Numerical Studies of the Drying of Hemp Concrete.” In *17th International Drying Symposium*. Magdeburg.

405 Grenelle 1 Enivronnement, 2015. 2010. “Le Grenelle 1 Enivronnement.”
406 http://www.side.developpement-durable.gouv.fr/userfiles/memento_maires.pdf.

407 Gualtieri, A. F., A. Ricchi, M. Lassinantti Gualtieri, S. Maretti, and M. Tamburini. 2016.
408 “Kinetic Study of the Drying Process of Clay Bricks.” *Journal of Thermal Analysis and*
409 *Calorimetry* 123 (1): 153–67. https://doi.org/10.1007/s10973-015-4868-6.

410 Hii, C. L., C. L. Law, and M. Cloke. 2009. “Modeling Using a New Thin Layer Drying Model and
411 Product Quality of Cocoa.” *Journal of Food Engineering* 90 (2): 191–98.
412 https://doi.org/10.1016/j.jfoodeng.2008.06.022.

413 ISO527-4. 1997. “ISO 527-4, Plastics — Determination of Tensile Properties — Part 4: Test
414 Conditions for Isotropic and Orthotropic Fibre-Reinforced Plastic Composites.”
415 https://www.iso.org/standard/4595.html.

416 Karaky, Hamzé. 2018. “Élaboration et Caractérisation Physique et Hygrothermique d’un
417 Agro-Matériau à Base de Pulpe de Betterave et d’amidon.” Université de Reims-
418 Champagne-Ardenne.

419 Karaky, Hamzé, Chadi Maalouf, Christophe Bliard, Alexandre Gacoin, Nadim El Wakil, and
420 Guillaume Polidori. 2019. “Characterization of Beet-Pulp Fiber Reinforced Potato Starch
421 Biopolymer Composites for Building Applications.” *Construction and Building Materials*.
422 https://doi.org/10.1016/j.conbuildmat.2019.01.127.

423 Karaky, Hamzé, Chadi Maalouf, Christophe Bliard, Tala Moussa, Nadim El Wakil, Mohammed
424 Lachi, and Guillaume Polidori. 2018. “Hygrothermal and Acoustical Performance of
425 Starch-Beet Pulp Composites for Building Thermal Insulation.” *Materials* 11 (9): 1622.
426 https://doi.org/10.3390/ma11091622.

427 Karathanos, Vaios T., and Vasilios G. Belessiotis. 1999. “Application of a Thin-Layer Equation
428 to Drying Data of Fresh and Semi-Dried Fruits.” *Journal of Agricultural and Engineering*
429 *Research* 74 (4): 355–61. https://doi.org/10.1006/jaer.1999.0473.

430 Karel, M. 1975. “Heat and Mass Transfer in Freeze Drying.” *Freeze Drying and Advanced*
431 *Food Technology*, 177–202.

432 Karoglou, Maria, A. Moropoulou, Z. B. Maroulis, and M. K. Krokida. 2005. “Drying Kinetics of
433 Some Building Materials.” *Drying Technology* 23 (1-2 SPEC. ISS.): 305–15.
434 https://doi.org/10.1081/DRT-200047926.

435 Khalfallah, M., B. Abbès, F. Abbès, Y. Q. Guo, V. Marcel, A. Duval, F. Vanfleteren, and F.
436 Rousseau. 2014. “Innovative Flax Tapes Reinforced Acrodur Biocomposites: A New
437 Alternative for Automotive Applications.” *Materials and Design* 64 (December): 116–26.
438 https://doi.org/10.1016/j.matdes.2014.07.029.

439 Lee, W H. 1979. “A Pressure Iteration Scheme for Two-Phase Flow Modeling.” Technical
440 Report LA-UR 79-975, Los Alamos, New Mexico.

441 LTECV. 2015. “LOI N° 2015-992.” 2015.
442 https://www.legifrance.gouv.fr/affichTexte.do?cidTexte=JORFTEXT000031044385&cate
443 gorieLien=id.

444 Masonry, Hollow Brick. 2008. “TECHNICAL NOTES on Brick Construction.”

Midilli, A., H. Kucuk, and Z. Yapar. 2002. “A New Model for Single-Layer Drying.” *Drying Technology* 20 (7): 1503–13. https://doi.org/10.1081/DRT-120005864.

Mnasri, Faiza, Sofiane Bahria, Mohamed El-Amine Slimani, Ouhsaine Lahoucine, and Mohammed El Ganaoui. 2020. “Building Incorporated Bio-Based Materials: Experimental and Numerical Study.” *Journal of Building Engineering* 28: 101088. https://doi.org/10.1016/j.jobe.2019.101088.

Niang, Ibrahim, Chadi Maalouf, Tala Moussa, Christophe Bliard, Etienne Samin, Céline Thomachot-Schneider, Mohamed Lachi, Hervé Pron, Ton Hoang Mai, and Salif Gaye. 2018. “Hygrothermal Performance of Various Typha–Clay Composite.” *Journal of Building Physics* 42 (3): 316–35. https://doi.org/10.1177/1744259118759677.

Onwude, Daniel I., Norhashila Hashim, Rimfiel B. Janius, Nazmi Mat Nawi, and Khalina Abdan. 2016. “Modeling the Thin-Layer Drying of Fruits and Vegetables: A Review.” *Comprehensive Reviews in Food Science and Food Safety* 15 (3): 599–618. https://doi.org/10.1111/1541-4337.12196.

Paquet Climat-Energie. 2008. “Conseil Européen.” Bruxelles. http://www.consilium.europa.eu/ueDocs/cms_Data/docs/pressData/fr/ec/104669.pdf.

RBR, and RBR 2020-2050. 2015. “PLAN BATIMENT DURABLE Groupe de Travail Réflexion Bâtiment Responsable 2020- 2050 (RBR 2020-2050).” http://www.planbatimentdurable.fr/IMG/pdf/Telecharger_la_note_RBR_2020-2050__BEPOS_PV_et_Systeme_electrique_-Septembre_2015.pdf.

RT. 2012. “La RT2012 : Un Saut Énergétique Pour Les Bâtiments Neufs - Ministère de l’Environnement, de l’Energie et de La Mer.” http://www.developpement-durable.gouv.fr/La-RT2012-un-saut-energetique-pour.html.

Schellbach, G. 1971. “The Influence of Perforation on the Load-Bearing Capacity of Hollow Brick Masonry Structures.” In *The Second International Brick Masonry Conference (Stoke-on-Trent)*.

Shahidzadeh-Bonn, N. Azouni, A., and P. Coussot. 2007. “Effect of Wetting Properties on the Kinetics of Drying of Porous Media.” *Journal of Physics: Condensed Matter* 19 (11).

Simal, S., A. Femenia, M. C. Garau, and C. Rosselló. 2005. “Use of Exponential, Page’s and Diffusional Models to Simulate the Drying Kinetics of Kiwi Fruit.” *Journal of Food Engineering* 66 (3): 323–28. https://doi.org/10.1016/j.jfoodeng.2004.03.025.

Sogi, D. S., U. S. Shivhare, S. K. Garg, and A. S. Bawa. 2003. “Water Sorption Isotherm and Drying Characteristics of Tomato Seeds.” *Biosystems Engineering* 84 (3): 297–301. https://doi.org/10.1016/S1537-5110(02)00275-1.

Taghian Dinani, Somayeh, Nasser Hamdami, Mohammad Shahedi, and Michel Havet. 2014. “Mathematical Modeling of Hot Air/Electrohydrodynamic (EHD) Drying Kinetics of Mushroom Slices.” *Energy Conversion and Management* 86 (October): 70–80. https://doi.org/10.1016/j.enconman.2014.05.010.

Vega, A., P. Fito, A. Andrés, and R. Lemus. 2007. “Mathematical Modeling of Hot-Air Drying Kinetics of Red Bell Pepper (Var. Lamuyo).” *Journal of Food Engineering* 79 (4): 1460–66. https://doi.org/10.1016/j.jfoodeng.2006.04.028.

Yaldiz, Osman, Can Ertekin, and H. Ibrahim Uzun. 2001. “Mathematical Modeling of Thin Layer Solar Drying of Sultana Grapes.” *Energy* 26 (5): 457–65. https://doi.org/10.1016/S0360-5442(01)00018-4.

VII. List of symbols

Symbol	Definition
L, L’	Length (m)
w, w’	Width (m)
h, h’	Height (m)
V	Volume (m^3)
∅	Diameter (m)
ρ	Density ($kg.m^{-3}$)
m	Mass (kg)
S	Shrinkage percentage (%)
MR	Mass ratio (-)
$\dot{m}$	Mass transfer rate ($kg.m^{-3}.s^{-1}$)
α_v	Volume fraction (-)
$\vec{V}$	Velocity ($m.s^{-1}$)